

Prediction of the radiative heat transfer in small and large scale oxy-coal furnaces



Xin Yang^a, Alastair Clements^a, János Szuhánszki^a, Xiaohong Huang^b, Oscar Farias Moguel^a, Jia Li^a, Jon Gibbins^a, Zhaohui Liu^b, Chuguang Zheng^b, Derek Ingham^a, Lin Ma^{a,*}, Bill Nimmo^a, Mohamed Pourkashanian^a

^a Energy 2050, Department of Mechanical Engineering, University of Sheffield, Sheffield S10 2TN, UK

^b State Key Laboratory of Coal Combustion, School of Energy and Power Engineering, Huazhong University of Science and Technology, Wuhan 430074, China

HIGHLIGHTS

- CFD modelling of radiation in small and large scale oxy-coal furnaces is developed.
- Effects of FSCK and Mie data on radiation are investigated and discussed.
- Non-grey modelling of gas radiation is enhanced in the large furnace.
- A hotter flame and a higher gas radiation are predicted through FSCK and Mie data.

ARTICLE INFO

Keywords:

CFD
Radiative heat transfer
Oxyfuel combustion
Radiation model

ABSTRACT

Predicting thermal radiation for oxy-coal combustion highlights the importance of the radiation models for the spectral properties of gases and particles. This study numerically investigates radiation behaviours in small and large scale furnaces through refined radiative property models, using the full-spectrum correlated k (FSCK) model and Mie theory based data, compared with the conventional use of the weighted sum of grey gases (WSGG) model and the constant values of the particle radiation properties. Both oxy-coal combustion and air-fired combustion have been investigated numerically and compared with combustion plant experimental data. Reasonable agreements are obtained between the predicted results and the measured data. Employing the refined radiative property models achieves closer predicted heat transfer properties to the measured data from both furnaces. The gas-phase component of the radiation energy source term obtained from the FSCK property model is higher within the flame region than the values obtained by using the conventional methods. The impact of using non-grey radiation behaviour of gases through the FSCK is enhanced in the large scale furnace as the predicted gas radiation source term is approximately 2–3 times that obtained when using the WSGG, while the same term is in much closer agreement between the FSCK and the WSGG for the pilot-scale furnace. The predicted total radiation source term (from both gases and particles) is lower in the flame region after using the refined models, which results in a hotter flame (approximately 50–150 K higher in this study) compared with results obtained from conventional methods. In addition, the predicted surface incident radiation reduces by using the refined radiative property models for both furnaces, in which the difference is relevant with the difference in the predicted radiation properties between the two modelling techniques. Numerical uncertainties resulting from the influences of combustion model, turbulent particle dispersion and turbulence modelling on the radiation behaviours are discussed.

1. Introduction

Oxyfuel combustion has been regarded as one of the most promising technologies for both new and existing power stations in order to achieve a near-zero CO₂ emission [1,2]. Under oxyfuel conditions, air is

replaced by the recycled flue gases (wet or dry) and high purity oxygen in order to control the combustion temperature and produce a high CO₂ concentration in the flue gas. Because of the differences in the thermal properties of the combustion gases (heat capacity and radiation properties), oxyfuel conditions lead to uncertainties in determining the

* Corresponding author.

E-mail address: lin.ma@sheffield.ac.uk (L. Ma).

<https://doi.org/10.1016/j.apenergy.2017.11.070>

Received 28 August 2017; Received in revised form 1 November 2017; Accepted 13 November 2017

0306-2619/© 2017 The Authors. Published by Elsevier Ltd. This is an open access article under the CC BY license (<http://creativecommons.org/licenses/by/4.0/>).

Nomenclature			
$A_{p,i}$	projected surface area of particle i (m^2)	θ_R	radiation temperature (K)
C_D	drag coefficient	κ	absorption coefficient (1/m)
C_L	time scale constant	κ_p	equivalent particle absorption coefficient (1/m)
c_p	specific heat at constant pressure (J/(kg·K))	μ	viscosity (kg/m·s)
d	diameter (m)	ρ	density (kg/m^3)
E	emission (W/m^3)	σ_p	equivalent particle scattering coefficient (1/m)
$f_{p,i}$	particle scattering factor	τ_e	eddy lifetime (s)
\vec{F}	an additional acceleration due to the other body forces (m/s^2)	ϕ	scattering phase function
g	asymmetry factor	Ω	solid angle (sr)
G	local incident radiation (W/m^2)	<i>Subscripts</i>	
h	convective heat transfer coefficient ($W/(m^2\cdot K)$)	b	black body
I	radiation intensity ($W/(sr\cdot m^3)$)	g	gas
k	kinetic energy (m^2/s^2)	p	particle
m	mass (kg)	λ	wavelength
$M_{w,i}$	molecular weight (kg/kmol)	<i>Abbreviations</i>	
n_i	number density of particles ($1/m^3$)	AD	air dried
q	radiative flux (W/m^2)	AR	as received
$Q_{abs,i}$	particle emissivity	CPD	chemical percolation devolatilization
Q_p	heat resulting from vaporization and chemical reactions (W)	CTF	combustion test facility
$Q_{sca,i}$	particle scattering efficiency	DAF	dry ash-free
r	uniform random number	DOM	discrete ordinates radiation model
\vec{r}	position vector	DPM	discrete phase model
Re	Reynolds number	DRW	discrete random walk
$R_{i,r}$	net rate of production of a species ($kmol/(m^3\cdot s)$)	EDM	eddy-dissipation model
\vec{s}	direction vector	EWB	exponential wideband
\vec{s}'	scattering vector	FSCK	full-spectrum correlated k
t	time (s)	FSK	full-spectrum k
T	temperature (K)	IRZ	internal recirculation zone
u'	velocity fluctuating component (m/s)	LBL	line-by-line
V	volume (m^3)	OFA	over fire air
$w_{p,i}$	particle emissivity weighting factor	ORZ	outer recirculation zone
Y_p	the time averaged mass fractions of the product species	RSM	Reynolds stress model
Y_R	the time averaged mass fractions of the reactant	RTE	radiative transfer equation
<i>Greek letters</i>		SLW	spectral-line-based weighted-sum-of-grey-gases
ε	turbulent dissipation rate (m^2/s^3)	SNB	statistical narrow-band
ζ	normally distributed random number	SWF	scalable wall functions
		TRI	turbulence-radiation interaction
		WSGG	weighted sum of grey gases

thermal conditions, which plays a critical role in determining the operation and scale-up of the combustors [3]. The role of increased CO₂ and H₂O concentrations on the transport of thermal radiation within the furnace is particularly challenging to predict, however, it is critical to have a detailed understanding of this impact, which will influence the temperature distribution inside the furnace, heat fluxes to the wall, pollutant formation and the flame shape [2,4,5].

Computational fluid dynamics (CFD) has been widely used for simulating combustion processes, and it has also been applied in the modelling of oxy-coal combustion (for the combustion and heat transfer behaviours [6–15], for the effects of oxyfuel conditions on retrofitting [8,9,11,15–19], for the large scale combustors [7–9,15,17,20], etc.). In order to achieve a better prediction of radiative heat transfer for oxy-coal combustion systems, especially for different oxyfuel conditions, such as oxygen concentrations and flue gas recycling ratios, an accurate estimation of the radiation properties of gases and particles needs to be integrated into the CFD modelling approach.

The absorption coefficients for triatomic molecules, such as CO₂ and H₂O, exhibit strong oscillations across the electromagnetic spectrum. However, quantities of interest, such as the net exchange of energy between the combustion medium and the intensity field, as well as the

total heat flux to the walls, require an integration of a function of this absorption coefficient across all wavelengths. Standard numerical approaches to resolve this integration, termed the line-by-line (LBL) approach, will typically require 10⁵–10⁷ discrete intervals, which is prohibitively large [21]. Recently, developments of the Monte Carlo method have been able to provide LBL accuracy within coupled combustion applications [22], however, it is still an active challenge to apply this approach to large-scale multi-phase applications. Narrow band models, such as the statistical narrow band (SNB) and correlated k models, are capable of reducing this burden to a few hundred intervals, however this is still too expensive for CFD approaches, which require the resolution of the radiation intensity field across a fine spatial and angular resolution [21,23]. Wide band models, such as the exponential wide band (EWB) model, further reduce the number of the band intervals [24], however these methods typically have much reduced accuracy over narrow band approaches [21,23,25] and still need to improve in its computational efficiency for the engineering applications [21,26]. Global models, such as the weighted sum of grey gases (WSGG) [27,28], spectral line-based WSGG (SLW) [29] and full spectrum correlated- k (FSCK) models [30], where the spectral integrity of the gas absorption is discarded in order to solve integral properties of

the intensity field, have been able to show narrow-band and LBL accuracy for practical cases with fewer than ten intervals in the surrogate spectral dimension [31]. From these models, the grey WSGG method has been widely adopted in CFD calculations due to its ability to demonstrate a composition dependent absorption coefficient within an acceptable time [27]. However, this method has long-known drawbacks in accuracy [32]. Recent developments of the WSGG model have focused on widening its applicability to oxyfuel conditions. Several refined WSGG models have been derived from more rigorous radiation models (exponential wideband, EWB; statistical narrow-band, SNB; LBL), have been proposed by Johansson et al. [33,34], Yin et al. [35,36], Kangwanpongpan et al. [37], and Bordbar et al. [38]. However, the refined WSGG models, which are developed based on pre-defined combustion conditions, could potentially be inflexible in novel combustion environments. The FSCK method used in this study has previously shown to provide good accuracy, compared to LBL data [39], as well as improved agreements to narrow band methods in air and oxyfuel conditions against WSGG models [31,40–42], and has therefore been chosen as a refined approach to modelling gas radiation properties.

Particle radiation is a significant factor in determining the thermal radiation heat transfer for solid fuel combustion. Johansson et al. [43] investigated the importance of particle and gas radiation in a simplified cylindrical geometry with a similar thermal radiation as in a 100 kW oxy-coal combustor through the Mie theory and SNB gas property model. It was found that the particle radiation dominates the total radiation for the small scale combustor. In addition, the dominant role of particle radiation in the total radiation for solid fuel combustion has been confirmed by Yin et al. [6,7] and Zhang et al. [44] through CFD simulations of large scale combustors while using the relatively simpler radiation model (the refined WSGG model for the gas radiation properties and carbon conversion-dependent values of the particle radiation properties).

Due to model availability and computational cost, the research on CFD simulation of real solid fuel combustors with the relatively more rigorous radiation models for the spectral properties of gases and particles (such as, FSCK and Mie data based methods) is limited. Development of these refined radiation models could provide a better understanding of the gas and particle radiation behaviours for oxyfuel combustion, making it very important to investigate the radiative heat transfer for these conditions in real small and large scale combustors. For the first time, the radiative heat transfer for oxy-coal combustion across different scaled furnaces is studied by using the refined radiation property models for both gas- and particle-phase components. Through comparing the predicted radiation behaviours between the refined radiation property models and the conventional methods (the WSGG model and the constant value of particle radiation properties), the differences in the prediction performance between these models are investigated and discussed, with the specific attention on how the modelling approaches affect the coupling to the energy field. The pilot-scale PACT 250 kW air/oxyfuel combustion test facility (CTF) can offer detailed analysis of the combustion process under air and oxyfuel combustion conditions [10]. The semi-industrial furnace (35 MW oxy-fuel boiler) in Yingcheng, which is lead by the Huazhong University of Science and Technology, is a compatible design facility capable of operating in both air and oxyfuel combustion conditions [18]. The experimental data from these two furnaces has been used to validate the modelling approach proposed in this study.

2. Source of experimental data

2.1. Pilot-scale furnace

The PACT 250 kW air/oxyfuel combustion test facility (CTF) is a single-burner down-fired cylindrical furnace, as shown in Fig. 1. It consists of eight refractory lined sections with an inner diameter of

0.9 m and an overall length of 4 m. The swirl burner, a scaled version of a commercially available Doosan Babcock Mark III low NOx burner, consists of a primary register through which the pulverized coal and the primary oxidiser stream at ambient temperatures are fed (air or a mixture of oxygen and carbon dioxide, depending on the mode of operation), and the secondary and tertiary inlets for delivering the rest of the preheated oxidiser. More details of the furnace and the burner can be found in [45,46]. Incident radiative heat transfer to the furnace walls has been measured using an IFRF ellipsoidal radiometer. The gold plated, ellipsoidal cavity of the probe focuses the radiation entering the probe tip onto the surface of a thermopile sensor to measure the incident radiation at the surface where the probe is inserted. A protective window within the cavity and a nitrogen purge are applied to shield the sensor from the effect of convection. Gas samples, which are collected within the furnace through a water cooled gas extraction probe, are measured by the Signal MAXSYS 900 Series gas analyser.

The operating conditions for the three different cases (including one air case and two oxyfuel cases) in this paper are shown Table 1. The two pilot scale oxyfuel cases have been tested with a total inlet oxygen concentration of 27% (Oxy27) and 30% (Oxy30) in order to obtain a similar temperature distribution and radiative heat transfer in the air-fired combustion conditions. The properties of the El-Cerrejon coal used for the experimental combustion cases are shown in Table 2.

2.2. Semi-industrial furnace

The 35 MW semi-industrial furnace used in this study is a large pilot-scale front wall-fired boiler. As shown in Fig. 2, it consists of three swirl burners and two over fire air (OFA) nozzles at the front wall. The swirl burner consists of a central nozzle (transporting a small quantity of oxidant stream in order to protect the oil pipe), a non-swirling primary register and a swirling secondary register. More details of the

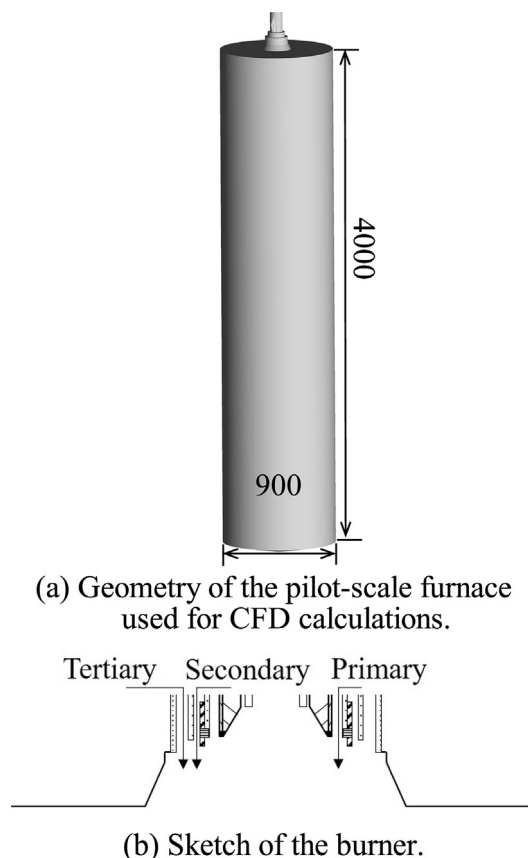


Fig. 1. Geometry of the pilot-scale furnace and the sketch of the burner (dimensions in mm).

Table 1
Summary of operation conditions of the pilot-scale furnace that were used for the CFD calculations (Air, Oxy27 and Oxy30).

	Air	Oxy27	Oxy30
<i>Mass flow rate (kg/h)</i>			
Fuel	25.7	25.7	25.7
Primary	60.1	60.9	54.8
Secondary	92.2	87.8	78.2
Tertiary	158.3	150.7	134.3
<i>Inlet gas temperature (K)</i>			
Primary	297	295	295
Secondary	525	525	525
Tertiary	525	525	525
<i>Oxygen concentration (vol.%)</i>			
Primary	20.84	21.00	21.00
Secondary	20.84	28.54	32.24
Tertiary	20.84	28.54	32.24

Table 2
Properties of El-Cerrejon coal.*

Proximate analysis (AR, wt.%)	Element analysis (DAF, wt.%)		
Fixed carbon	53.97	C	80.92
Volatiles	35.50	H	5.12
Ash	2.90	N	1.65
Moisture	7.63	S	0.52
NCV(MJ/kg)	28.41	O (by difference)	11.79

* AR, as received; DAF, dry ash-free.

Table 3
Summary of the operation conditions for the semi-industrial furnace that were used for CFD calculations (Air and Oxy28).

	Air	Oxy28
<i>Mass flow rate (t/h)</i>		
Fuel	4.68	4.46
Primary	7.94	8.37
Secondary	28.68	29.53
OFA	6.78	–
<i>Inlet gas temperature (K)</i>		
Primary	393	385
Secondary	517	507
OFA	342	–
<i>Species concentration of primary inlet (vol.%)</i>		
O ₂	21.00	19.17
H ₂ O	0	9.55
CO ₂	0	52.99
N ₂	79.00	18.29
<i>Species concentration of secondary inlet (vol.%)</i>		
O ₂	21	29.18
H ₂ O	0	13.79
CO ₂	0	42.08
N ₂	79	14.95

furnace and the burners can be found in [18]. The heat transfer to the furnace walls has been evaluated by measuring the temperatures of the water and steam in the membrane wall and the superheater. The in-furnace temperature has been measured using an OMEGA radiation thermometer. An oxygen level of 28% was chosen for the oxyfuel combustion case since this level could obtain a similar temperature distribution and heat transfer profile when using oxygen levels between

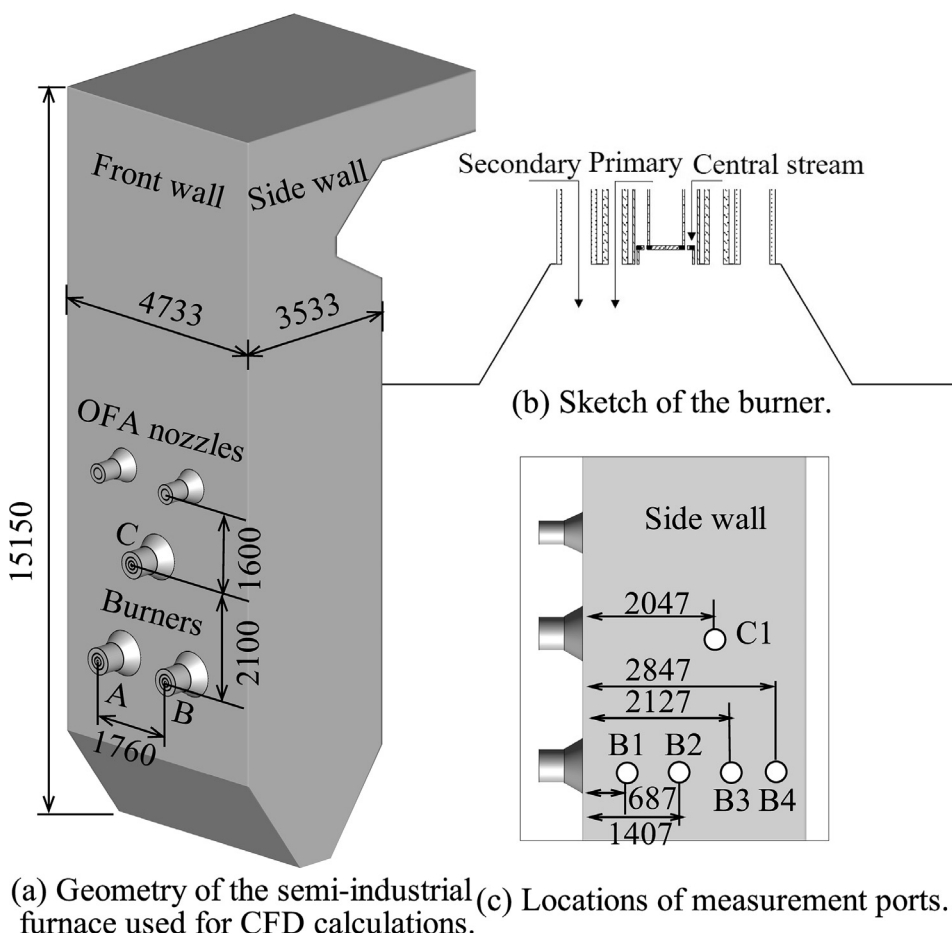


Fig. 2. Schematic configurations of the semi-industrial furnace (dimensions in mm): (a) geometry of the furnace used in the CFD calculations, (b) sketch of the burner, and (c) locations of the ports for the temperature measurements.

27% and 29% compared to the air-fired combustion condition through the theoretical reaction equilibrium calculation [18]. The operating conditions for the two different cases are shown in Table 3, and the properties of the Chinese coal used in this paper are shown in Table 4.

3. Mathematical models

3.1. Turbulence

The Reynolds Stress Model (RSM) using the linear pressure strain term and constants proposed by Gibson and Launder [47] has been employed to obtain an anisotropic turbulence closure of the Reynolds stresses, which makes the RSM potentially suitable for predicting highly swirling flows in combustors [48–51]. Scalable wall functions (SWF) are used to predict the velocity and temperature distributions at the nearest grid from the wall surface with the benefit of avoiding having to refine the boundary layer, while maintaining numerical stability in grid locations that are close to the wall.

3.2. Radiation heat transfer

Radiation heat transfer, which is the dominant factor in determining the heat transfer in boilers, is modelled by solving the radiative transfer equation (RTE). In terms of a non-grey gas mixture (absorbing and emitting, without scattering) with grey particles (absorbing, emitting and scattering), the RTE for the spectral intensity $I_\lambda(\vec{r}, \vec{s})$ can be written as:

$$\frac{dI_\lambda(\vec{r}, \vec{s})}{ds} = \kappa_{g,\lambda} I_{b,\lambda} + E_p - (\kappa_{g,\lambda} + \kappa_p + \sigma_p) I_\lambda(\vec{r}, \vec{s}) + \frac{\sigma_p}{4\pi} \int_0^{4\pi} I_\lambda(\vec{r}, \vec{s}') \phi(\vec{s} \cdot \vec{s}') d\Omega \quad (1)$$

where λ is the wavelength, \vec{r} , \vec{s} and \vec{s}' are the position vector, direction vector and scattering direction vector, respectively; $\kappa_{g,\lambda}$ is the gas spectral absorption coefficient, $I_{b,\lambda}$ is the black body intensity given by the Planck function; $\phi(\vec{s} \cdot \vec{s}')$, which is the scattering phase function, is considered to be isotropic in this work and therefore equal to unity. E_p is the equivalent particle emission, κ_p and σ_p are the equivalent particle absorption and scattering coefficients over a given volume V , as follows:

$$E_p = \frac{1}{V} \sum_i Q_{abs,i} A_{p,i} w_{p,i} I_b(T_{p,i}) \quad (2)$$

$$\kappa_p = \frac{1}{V} \sum_i Q_{abs,i} A_{p,i} \quad (3)$$

$$\sigma_p = \frac{1}{V} \sum_i Q_{sca,i} A_{p,i} \quad (4)$$

where $Q_{abs,i}$ is particle absorption efficiency, which is the same as the particle emissivity, $Q_{sca,i}$ is the particle scattering efficiency, $A_{p,i}$ is the projected surface area of particle i , $I_b(T_{p,i})$ is the blackbody emission evaluated at the particle temperature, and $w_{p,i}$ is an emissivity weighting factor that appropriately weights the particle emission into the band represented in Eq. (1). The particle absorption and scattering efficiencies can be calculated using the Mie theory, however, in order to use Mie theory calculated scattering efficiencies with an isotropic phase function, it is necessary to remove the forward scattering directions by using the modified scattering efficiency Q_{sca}^* [52], which is calculated as:

$$Q_{sca}^* = Q_{sca}(1-g) \quad (5)$$

where g is the asymmetry factor calculated from Mie theory. For comparison, constant particle radiative properties using a particle absorption efficiency of 0.9 and a value of 0.6 for the scattering factor, f_p , was chosen, as used previously by [18]. The scattering efficiency is

calculated from the given scattering factor of the particle as:

$$Q_{sca} = (1-f_p)(1-Q_{abs}) \quad (6)$$

resulting in a scattering efficiency of 0.04 for the constant particle properties. The radiation heat transfer is included into the energy equation through a source term, S_{rad} , which can be described by the divergence of the radiative flux, $q_\lambda(\vec{r})$, and defined as the net change in intensity across a volume as follows:

$$\nabla \cdot q_\lambda(\vec{r}) = \underbrace{\kappa_{g,\lambda} \left[4\pi \frac{\sigma T_g^4}{\pi} - \int_0^{4\pi} I_\lambda(\vec{r}, \vec{s}) d\Omega \right]}_{\text{Gas radiation source, } S_{grad}} + \underbrace{\left[4\pi E_p - \kappa_p \int_0^{4\pi} I_\lambda(\vec{r}, \vec{s}) d\Omega \right]}_{\text{Particle radiation source, } S_{prad}} \quad (7)$$

The accuracy of predicting the thermal radiation is highly dependent on the method used to solve the RTE and the models to predict the radiation properties of the media. The discrete ordinates radiation model (DOM), which has a potential to achieve a balance between accuracy and computational time [48], is widely used for modelling radiation for solid fuel combustion in CFD. The DOM solves the RTE for a finite number of discrete directions ($=N_\theta \times N_\phi$) at each octant of the angle range by using a finite volume approach. The accuracy of the DOM is dependent on the discretisation for the octant angle. The predicted results of the incident radiation on the wall by using the DOM with a 3×3 angular discretisation are similar to those when employing a 4×4 angular discretisation for both pilot-scale furnace and semi-industrial furnace. Therefore, the 3×3 angular discretisation is employed, which resulted in 72 ordinates for the DOM in this study.

The absorption coefficient of the gas mixture is predicted by the FSK model, which is based on a reordered absorption coefficient against a normalised spectral dimension [39,53]. The FSK model predicts the absorption efficiency from the inverse function of the cumulative k -distribution, where the k -distribution represents the accumulated frequency of the absorption coefficient weighted by the Planck function. The total radiative intensity is integrated through an efficient Gauss quadrature scheme due to the smooth nature of the cumulative k -distribution. A five-point Gauss quadrature has been chosen since its prediction performance is similar to the higher discretisation for oxy-fuel conditions [10,31]. More details of the FSK model can be found in [10,31,39,53]. In addition, the traditional grey WSGG model, which predicts the absorption coefficient based on the weighted sum of emissivity from fictitious grey gases, is used to predict the gas absorption coefficient in order to compare with the FSK model. In terms of the computational efficiency, the computational time and the required memory for the FSK model are about 1.5 times and 3.3 times the requirements of the WSGG model in this study, respectively.

Planck averaged particle radiative properties (emissivity and scattering efficiency) are predicted based on the Mie theory with the assumption of spherical particles, using the method by Bohren and Huffman [54]. For fuel and char particles, the measured spectrally variable optical constants from Manickavasagam et al. [55] were employed and the resulting emissivity and scattering efficiencies are in the range 0.9–1.2 and 0.1–0.2, respectively. For fly ash particles, the optical

Table 4
Properties of the Chinese coal.*

Proximate analysis (AD, wt.%)		Element analysis (AD, wt.%)	
Fixed carbon	49.81	C	60.40
Volatiles	23.77	H	3.65
Ash	23.94	N	0.48
Moisture	3.38	S	0.85
NCV(MJ/kg)	23.33	O	7.30

* AD, air dried.

constants from Goodwin et al. [56] were employed through the tabulation from Liu et al. [57] and the emissivity and scattering efficiencies are in the range 0.1–1.1 and 0.1–0.4, respectively. For burning char particles, the optical constants were calculated through a linear interpolation between the optical properties of coal and fly ash particles. Fig. 3 shows the Mie data based particle emissivity and scattering efficiency for the particles with the mean diameters of 120 μm and 45 μm as a function of particle temperature. Grey particle emissions are included in the non-grey FSCK model by scaling the radiative source through the emissivity weight function evaluated at the particle temperature, while grey particle absorption was added to the local k-distribution values [10]. The emissivity for char particles in the Mie data is close to that of the constant value used in this study, while the emissivity for ash particles is quite different between the Mie data and the constant value.

Soot radiation is neglected in this study due to the difficulty in accurately modelling soot formation and its radiation behaviour for coal flames under different combustion conditions. Neglecting soot radiation interaction may lead to predicting a higher temperature profile in the flame region [58,59]. However, from previous findings by [10,45], where the radiation from the soot is taken into account by using the soot models derived by Brown and Fletcher [59], the difference in predicting the radiation behaviour with soot radiation is insignificant compared to the results obtained without soot radiation. Hence, a robust model in predicting the formation of coal derived soot and its radiation properties is required to model the soot radiation with more confidence. In addition, turbulence-radiation interaction (TRI), which affects the prediction of the radiation intensity and the radiation source term, is neglected in this study. The radiative heat transfer could be underestimated without taking into consideration the TRI for the turbulent gas combustion [60,61]. However, for coal combustion systems, the effect of TRI on predicting radiation could be reduced by modelling the particles through the Lagrangian particle tracking method along with the Discrete Random Walk (DRW) model [40], where the turbulent fluctuation in the particle properties (particle temperature, particle dispersion, etc.) has been resolved. Up to date, it is still a challenge to accurately predict the TRI, which is highly dependent on the accurate modelling of turbulent structures, radiation properties, and turbulence-chemistry interaction.

3.3. Combustion models

Combustion of coal particles can be described by the sequential processes of inert heating, moisture release, devolatilisation, char combustion, and finally inert heating/cooling of ash particles. The same combustion models (devolatilization model and char combustion model) with model constants from Refs. [10,18], where the same coals are combusted in similar conditions, are employed in this study. The single kinetic rate model was employed for the devolatilization of the El-Cerrejon coal [10], where the rate of devolatilization depends on both the temperature and the remaining volatile content of the particles. The chemical percolation devolatilization (CPD) model was employed for the devolatilization of the Chinese coal [18]. Char combustion was modelled with the intrinsic char combustion model for the El-Cerrejon coal and the kinetic/diffusion-limited rate model for the Chinese coal [10,18]. The same values of the model constants have been employed for both the air-fired and oxyfuel combustion investigations.

The trajectories of the coal particles, which are modelled in a Lagrangian reference frame, are governed by the particle motion equation, which is a balance of the drag, gravity, and other body forces as formulated in the following equation:

$$\frac{d\vec{v}_p}{dt} = \frac{18\mu_g C_D Re_p}{\rho_p d_p^2} (\vec{v}_g - \vec{v}_p) + \frac{\vec{g}(\rho_p - \rho_g)}{\rho_p} + \vec{F} \quad (8)$$

where \vec{v} , ρ , μ and d are the velocity, density, viscosity and diameter of

the particles, respectively; the subscripts p and g refer to the particle and gas, respectively, C_D is the drag coefficient, and \vec{F} is an additional acceleration due to the other body forces, such as the virtual mass force and thermophoretic force. The virtual mass force, which is due to the acceleration of the fluid around the particle, can be ignored when the density of the particle is much greater than the density of the fluid. The thermophoretic force, which is significant for modelling ash deposition formation on the cold wall surfaces [62,63], is often neglected for predicting the combustion behaviour.

The effect of fluid turbulence on the particle trajectories has been considered by the Discrete Random Walk model (DRW), which integrates the particle motion equation of a sufficient number of particles using the instantaneous fluid velocity, \vec{u} (composed of the time-mean and fluctuating components, \bar{u} and u'), rather than the mean fluid velocity [48]. The fluctuating component (u') that prevails during the lifetime of the turbulent eddy is assumed to obey the Gaussian probability distribution function [48]. For RSM with nonisotropy of the stresses, the fluctuating component can be defined as:

$$u'_i = \zeta \sqrt{u_i'^2} \quad (9)$$

where i refers to the x, y, z directions and ζ is a normally distributed random number. The particles are assumed to interact with a succession of turbulent eddies. The particle-eddy interaction time in an eddy, which represents the frequency that the instantaneous velocity needs to be updated by applying a new value of ζ , is described by the smaller of the eddy lifetime (τ_e) and the eddy crossing time (t_{cross}), as follows:

$$\tau_e = -T_L \ln(r) \quad (10)$$

$$t_{cross} = -\frac{\rho_p d_p^2}{18\mu_g} \ln \left[1 - \left(\frac{18\mu_g L_e}{\rho_p d_p^2 |u_r|} \right) \right] \quad (11)$$

where $T_L = C_L \frac{k}{\epsilon}$, $L_e = \sqrt{2/3} \cdot C_L \frac{k^{1.5}}{\epsilon}$; C_L is the time scale constant, r is the uniform random number greater than zero and less than 1, u_r is the relative velocity between the gas and particle, and k and ϵ represent the turbulent kinetic energy and the dissipation rate, respectively. The prediction of particle dispersion rate by DRW is highly dependent on the value of the time scale constant, C_L , which is related to the turbulent

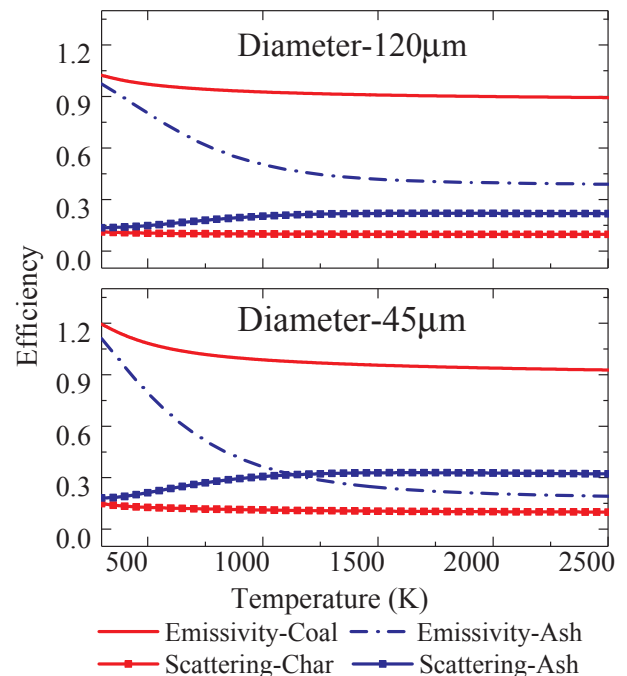


Fig. 3. Mie data based particle emissivity and scattering efficiency for the particles with the mean diameters of 120 μm and 45 μm as a function of particle temperature.

scales. A higher value of the time scale constant results in a higher particle dispersion rate. Generally, the value ranges from 0.15 to 0.6 according to the matched modelling results of the particle dispersion with the experimental data [64,65]. A typical value of 0.3 is employed for the RSM [48].

The energy balance equation of the particles, which is dictated by the convective heat transfer, the absorption/emission of radiation at the particle surface, and the latent heat or the heat of reaction, is given as follows:

$$m_p c_p \frac{dT_p}{dt} = hA_p(T_\infty - T_p) + \varepsilon_p A_p \sigma (\theta_R^4 - T_p^4) - Q_p \tag{12}$$

$$\theta_R = \left(\frac{G}{4\sigma} \right)^{1/4} \tag{13}$$

where m_p , c_p , T_p , A_p , and ε_p are the mass, specific heat, temperature, surface area and emissivity (equal to Q_{abs}) of the particles, respectively; T_∞ is the gas temperature, σ is the Stefan–Boltzmann constant, and θ_R is the radiation temperature; Q_p is the heat resulting from vaporization and chemical reactions; G is the local incident radiation.

The eddy-dissipation model (EDM), which assumes the turbulent mixing rate of reactant and product species controls the overall reaction rate [66], is widely used to model the gas phase combustion of volatile species and CO due to its simplicity and good convergence along with the reasonable accuracy. The net rate of production of a species is taken to be the smaller of the two expressions (reactant dissipation and product dissipation) as follows:

$$R_{i,r} = \min \left\{ \underbrace{\nu'_{i,r} M_{w,i} A \rho_s \frac{\varepsilon}{k} \min_R \left(\frac{Y_R}{\nu'_{R,i} M_{w,R}} \right)}_{\text{Reactant dissipation}}, \underbrace{\nu''_{i,r} M_{w,i} A B \rho_s \frac{\varepsilon}{k} \frac{\sum_P Y_P}{\sum_j \nu''_{j,r} M_{w,j}}}_{\text{Product dissipation}} \right\} \tag{14}$$

where $\nu'_{i,r}$ and $\nu''_{i,r}$ are the stoichiometric coefficient of reactant i and product j in reaction r , $M_{w,i}$ is the molecular weight, Y_R and Y_P are the time averaged mass fractions of reactant and product species; A is an empirical constant related to the turbulent scale in the flame region; B is an empirical constant with a value of 0.5, which is used to take into account the turbulent premixed flame. Therefore, for the coal diffusion flame, the empirical constant A may need to be verified according to the turbulent structure while the empirical constant B can be taken to be a constant value of 0.5. Visser et al. [67] optimized the value of the constant A for a swirling coal diffusion flame in a semi-industrial IFRF furnace by adjusting the prediction results of the gas species to the experimental data. Therefore, the recommended values of the constant A from Visser et al. [67], which are 0.5 and 0.7 for volatile and CO combustion respectively, are employed in this study.

3.4. Case set-up

In order to fully understand the contribution of gas radiation and particle radiation and compare the radiation models, 15 cases ($3 \times 3 + 2 \times 3$ conditions) have been numerically investigated, as shown in Table 5, among which the only differences are either combustion conditions (three combustion conditions for the pilot-scale furnace, as shown in Table 1; two combustion conditions for the semi-industrial furnace, as shown in Table 3) or the gas and particle radiation properties. A summary of the models and parameters that are employed in the simulations is given in Table 6. Fixed temperature boundary conditions have been employed for the furnace walls (approximately 350 K) for the pilot-scale furnace and the heat exchanger tube walls (approximately 600 K for the furnace wall and 720 K for the superheater wall) for the semi-industrial furnace, which are estimated by the temperature of the cooling water for the pilot-scale furnace and the saturation temperature of the steam for the semi-industrial furnace. A

typical internal emissivity of 0.8 is used for the pilot-scale furnace refractory materials [46], and 0.45 is used for the semi-industrial furnace which is installed with new tubes without ash deposition [18].

Hexahedral structured meshes have been used for the two furnaces based on the geometries presented in Figs. 1 and 2, where the effect of the swirl veins in the burners were taken into consideration by specifying the swirl numbers at the inlet [10,18]. The average gas temperature along the furnace height is used as the criteria of the grid independent study. For the pilot-scale furnace, a mesh with approximately 0.6 million cells for one quarter of the geometry is employed since its performance is similar to the finer meshes according to a grid independent study on three different meshes consisting of 0.6, 1.0 and 1.5 million cells. For the semi-industrial furnace, a mesh with about 4.2 million cells for the whole geometry is employed since its performance is similar to the finer mesh according to a grid independent study on three different meshes consisting of 2.2, 4.2 and 5.2 million cells.

4. Results and discussions

In this section, CFD predictions are compared with the experimental data of the combustion and radiation behaviours in the two furnaces. The effects of the refined radiation property models on predicting the radiation behaviours have been analysed and compared with the conventional radiation property models. In particular, the numerical uncertainties in predicting radiative heat transfer are discussed.

4.1. Pilot-scale furnace

4.1.1. Combustion behaviours

Fig. 4 shows a comparison of the gas species distribution close to the burner between the measured and predicted results for the air and oxyfuel cases in the 250 kW pilot-scale furnace. Generally, it is found that there exist minor differences in the gas species distribution by using the FSCK model and the Mie data compared with the results obtained by using the other two types of radiative property models. These minor differences in the species distributions could be attributed to the differences in the prediction results of the gas temperature distribution through using the different radiative property models. At the nearest measurement port to the burner exit, at an axial distance of 0.075 m, a higher concentration of CO₂ and a lower concentration of O₂ are experimentally observed within 0.1 m from the furnace centre compared to those at the radial distance of 0.13 m from the furnace centre, which results from the internal recirculation zone (IRZ) and is where the most intense combustion occurs. The concentration of CO₂ is lower along with a higher O₂ concentration, at a radial distance approximately 0.13 m from the furnace centre, where the main stream (secondary and tertiary streams) enters the combustion zone. From an outer radial distance of 0.2 m from the furnace centre, a higher concentration of CO₂ and a lower concentration of O₂ occur, which is related to the combustion gases being recirculated by the strong outer recirculation zone (ORZ). As shown in Fig. 4(b) and (c), at the axial

Table 5
Different cases investigated based on the radiation properties.

Radiation properties: Gas + Particle	Case				
	Pilot-scale furnace (C _p)			Semi-industrial furnace (C _i)	
	Air (1#)	Oxy27 (2#)	Oxy30 (3#)	Air (1#)	Oxy28 (2#)
WSGG + Constant (#1)	C _p 11	C _p 21	C _p 31	C _i 11	C _i 21
FSCK + Constant (#2)	C _p 12	C _p 22	C _p 32	C _i 12	C _i 22
FSCK + Mie (#3)	C _p 13	C _p 23	C _p 33	C _i 13	C _i 23

Table 6
Models and parameters used in the simulations.

Models	Descriptions
Turbulence	Reynold Stress Model (RSM) with scalable wall functions (SWF).
Radiation	Solution method: Discrete Ordinate model (DOM) with a 3×3 angular discretisation; Gas radiation properties: FSCK model and Smith's WSGG model; Particle radiation properties: Mie theory and constant values (emissivity, 0.9; scattering factor, 0.6).
Particle combustion	Particle trajectories: Discrete Phase Model (DPM) with Discrete Random Walk (DRW) model for turbulent dispersion, time scale constant = 0.3 and number of tries = 10; Particle size: Rosin-Rammler distribution with 10 size distributions; the mean diameter and the spread parameter are 120 μm and 1.1 for El-Cerrejon coal, and 45 μm and 2.5 for Chinese coal. Devolatilisation: Single kinetic rate model for El-Cerrejon coal, $A = 14841$, $E = 3.53 \times 10^7 \text{ J/kmol}$; CPD model for Chinese coal, the initial fraction of bridges in coal lattice = 0.64, initial fraction of char bridges = 0, lattice coordination number = 5.11, cluster molecular weight = 284.20 kg/kmol, and side chain molecular weight = 28.70 kg/kmol; Swelling coefficient = 1.1. Char combustion: The intrinsic char combustion model for the El-Cerrejon coal, mass diffusion-limited rate constant = 5.025×10^{-12} , kinetics-limited rate pre-exponential factor = 0.0004, kinetics-limited rate activation energy = $6.6 \times 10^7 \text{ J/kmol}$, Char porosity = 0.5, mean pore radius = $6 \times 10^{-8} \text{ m}$, specific internal surface area = $1 \times 10^5 \text{ m}^2/\text{kg}$, tortuosity = $\sqrt{2}$, burning model = 0.25; Kinetics/diffusion-limited combustion model, mass diffusion-limited rate constant 6.5×10^{-12} , kinetics-limited rate pre-exponential factor = 14.8, and kinetics-limited rate activation energy = $7.1 \times 10^7 \text{ J/kmol}$.
Gas phase combustion	Eddy-dissipation model (EDM) with a two-step reaction mechanism: Constant $A = 0.5$ and 0.7 for volatile and CO combustion, respectively, and Constant $B = 0.5$ for both combustions.

location of 0.075 m, it can be observed that the CO_2 concentration is under-predicted at the inner radial position for both oxyfuel cases, which may be attributed to the underestimation of the intensity of the inner recirculation zone through the RANS method [10]. In addition, the predicted CO concentration is much lower than the experimental data for all cases at the axial locations of 0.2 and 0.575 m, especially in the central region of the flame, which could be attributed to the neglect of both the char gasification reaction and the dissociation of the CO_2 . Also, this could lead to a less accurate prediction of the O_2 and CO_2 concentrations. With an increase in the axial distance from the burner exit, the variance of both the CO_2 and O_2 profiles gradually becomes flatter along the radial distance, as shown in both the predicted results and experimental data. This is because gases from the IRZ are mixing with the main stream along with consuming O_2 and producing CO_2 as the axial distance from the burner exit increases and the resulting gas concentrations gradually become closer to those recirculated at the ORZ.

Fig. 5 shows the predicted gas temperature distribution for the air and oxyfuel cases through the application of different radiation property models. The first observation is that higher gas temperatures are predicted with increasing oxygen levels for the oxyfuel cases and this is because of the enhanced fuel burning rates and lower gas velocities. Secondly, in terms of the radiative property models, it is observed that the predicted gas temperature when using the Mie data is higher than that with constant particle radiation properties (approximately 100–150 K higher at the internal recirculation zone), while the predicted gas temperature with the FSCK model is very similar to the result with the WSGG model.

4.1.2. Radiation

Fig. 6 shows the calculated radiation source terms (both gas and particle phases) along the furnace height by using different radiative property models. Peak values of the radiation source terms are observed in the flame region for all of the cases investigated. This is because the furnace temperature increases with the heat release increasing thermal radiation in the combustion region. It can be found that there is no clear difference in the predicted radiation source terms between the WSGG model and the FSCK model when the constant particle radiation property is used. In addition, particle radiation plays a major role in determining the total radiation (gases and particles) when the constant particle radiation property is used (particularly within the flame region). However, the particle radiation source term significantly drops (approximately by 50%) in the flame region when the Mie data based particle radiation properties are employed. This can be attributed to the

predicted particle absorption coefficient, when using the Mie theory data, being much lower than that calculated from using the constant value for the particle radiation property since ash particles are prescribed a much lower emissivity in the Mie theory data than the constant value. Interestingly, the predicted gas radiation source term is increased (approximately by two times in the flame region) when changing the particle radiation property to the Mie data based method, even though the same FSCK model is employed, compared with the other case when using the FSCK model and the constant particle radiation property based methods. This could be because the gas temperature distributions are different for the two cases, as the convective heat transfer between the ash particles and the gas increases, and this could correspondingly affect the gas radiation behaviour although the same gas radiative property model is employed. Generally, through the FSCK model and the Mie data based particle radiation property, a lower total radiation of gases and particles (resulting from a higher gas radiation and a lower particle radiation) are obtained in the flame region, which results in a hotter central region in the flame.

Fig. 7 shows a comparison of the measured and predicted surface incident radiation on the furnace wall by using different radiative property models. The predicted results of the surface incident radiation show reasonable agreements compared to the experimental data, where the trend of the predicted surface incident radiation is similar to that observed in the experimental data. Employing the refined radiative property models (FSCK and Mie theory based data) shows a lower surface incident radiation (reduced by approximately 5% in the flame region) compared to that obtained by using the conventional methods, which results in a closer predicted surface incident radiation to the measured data. Also, it is found that higher surface incident radiation occurs when changing from Oxy27 to Oxy30 in both the predicted and experimental data. This can be attributed to the higher gas temperature for the Oxy30 case, which results from the higher oxygen concentration and higher gas residence times in the furnace. It should be noted that there is a distinctly higher predicted surface incident radiations for both oxyfuel cases, while a closer predicted surface incident radiation is obtained for the air-fired combustion case. This could be attributed to the difficulty of using the same model constants when modelling the combustion (such as, the char combustion model and the homogeneous combustion model) derived from the air combustion conditions to accurately predict the oxyfuel combustion behaviours.

4.2. Radiation in the semi-industrial furnace

Fig. 8 shows the predicted gas temperature distribution for the air

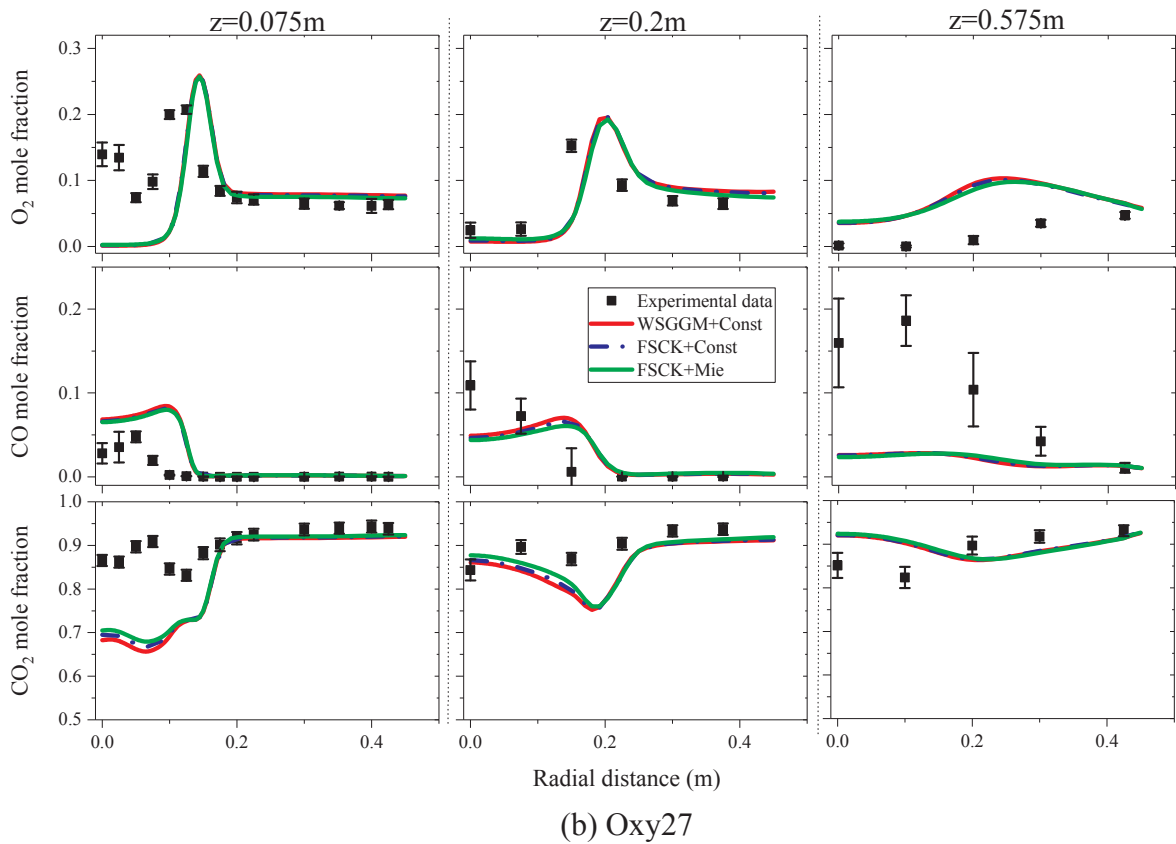
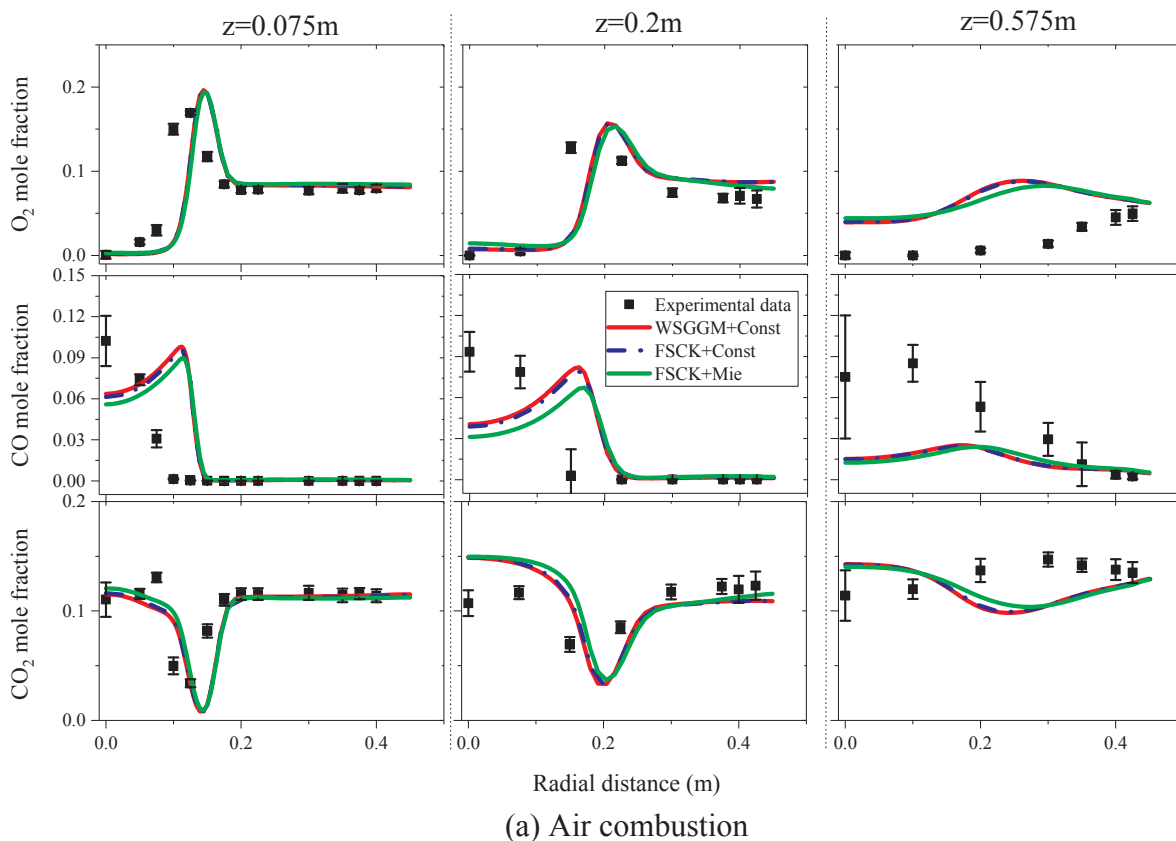


Fig. 4. Distribution of the measured and predicted gas species close to the burner ($z = 0.075\text{ m}$, 0.2 m and 0.575 m) by using different radiative property models: z represents the axial distance from the quartz exit; (a) Air combustion, (b) Oxy27 and (c) Oxy30.

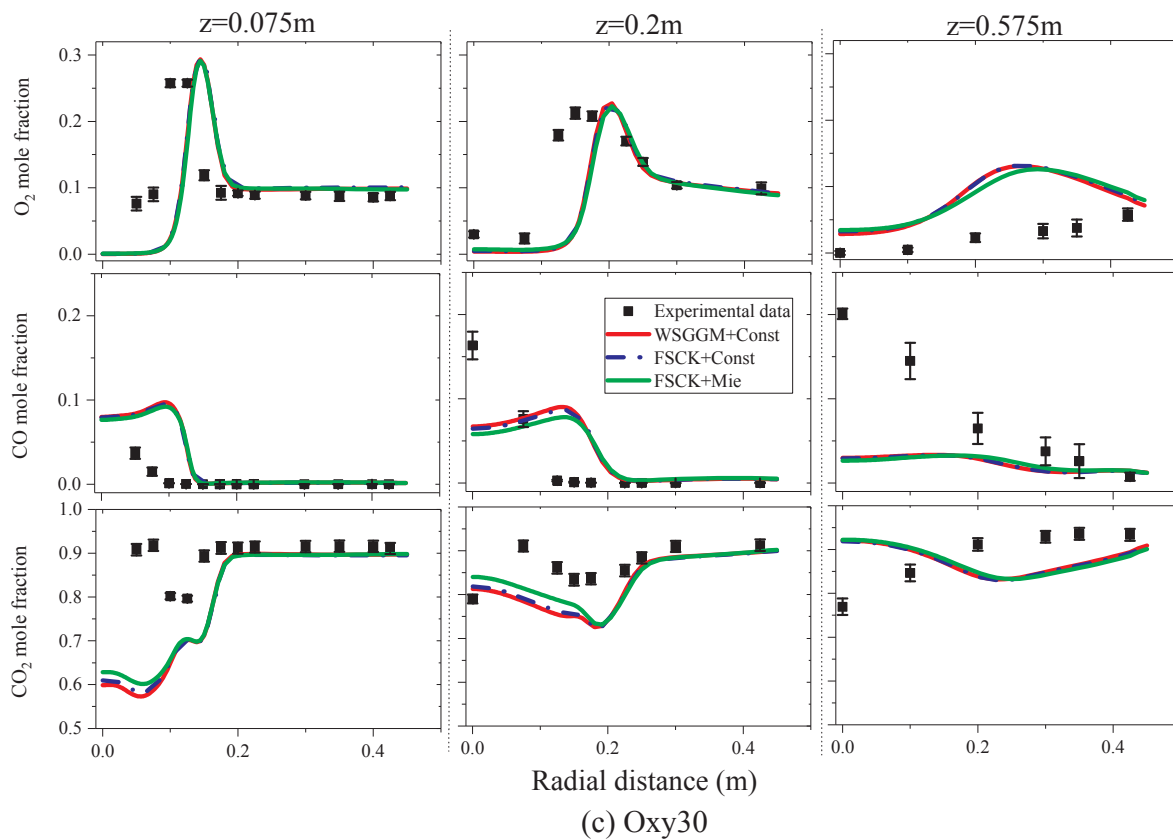


Fig. 4. (continued)

and oxyfuel cases when using different radiative property models. Fig. 9 shows the measured and predicted temperatures at the different measurement ports in the semi-industrial furnace for the air and oxyfuel cases. Generally, reasonable agreements between the experimental data and predictions are obtained, as shown in Fig. 9. The predicted gas temperature when using the FSCK model is higher than the temperature when using the WSGG model and a further slight increase in the gas temperature is observed after using the Mie data combined with the FSCK model, as shown in both Figs. 8 and 9. This is consistent with the prediction results where there is a decrease in the total radiation source term after using the refined radiation property models, as shown in Fig. 10. In addition, it can be observed that the predicted gas temperature under the oxyfuel combustion condition is slightly higher than that under the air-fired combustion condition. However, a slight decrease in the peak gas temperature in the flame region (ports B1, B2 and C1) is experimentally observed under the oxyfuel combustion condition compared to that under the air case. The difference in the trend of the peak gas temperature in the flame region between the prediction results and the experimental data could be due to the simplification in the combustion modelling, where the same model constants have been employed to simulate the combustion behaviours for both the air and oxyfuel conditions. In addition, the average gas temperatures (ports B3 and B4) are higher under the oxyfuel combustion condition than the air-fired combustion condition, which may result from the delayed combustion due to the influence of the CO_2 on the combustion rate and fluid heat capacity [46]. It should be noted that the difference in the predicted gas radiation behaviour between the FSCK model and the WSGG model is enhanced for the semi-industrial boiler, where the predicted gas temperature when using the FSCK model is approximately 50 K higher than the temperature when using the WSGG model in the flame region, as shown in Figs. 8 and 9. However, the influence of using the FSCK model on the predicted gas radiation behaviour is very small (only approximately 10 K difference in the predicted gas temperature in

the flame region) for the pilot-scale furnace. This overall effect could be due to the differences in the combustion conditions in the two furnaces along with an increased mean beam length of the semi-industrial furnace (approximately 1.60 m) compared with that of the small scale furnace (approximately 0.72 m). In addition, there is no clear difference in the predicted gas temperature distribution between the cases when using the Mie data based method and the constant particle radiative property model, which can be attributed to the similarly predicted particle radiation behaviour for the current cases.

Fig. 10 shows the predicted area averaged gas and particle radiation source terms along the furnace height by using different radiative property models. Two peak values are observed in the flame region close to the burners A + B and the burner C for all of the cases due to the heat release in the combustion region. Also, it is observed that there is a sharp reduction in both the gas and particle radiation source terms for the air combustion cases in the OFA region where the cool over fire air is injected, which results in a decrease in both the furnace temperature and the radiation emission. It is noticed that the gas radiation source term predicted by using the FSCK model is clearly higher (approximately 2–3 times in the flame region) than that from the WSGG model when the constant particle radiation property is used, which is in contrast from the cases in the pilot-scale furnace where there is no clear difference between the FSCK model and WSGG model. This can be explained by the effect in the difference in the gas absorption coefficient being amplified in the large scale furnace, which implies the importance of the non-grey modelling of the gas radiation is enhanced in the large scale furnace. It should be noted that the predicted particle radiation source term is also changed (approximately 30% lower in the flame region) even though the same constant particle radiation property is used, see Fig. 10. This is because the predicted gas temperature distributions are different between the two cases and this could correspondingly affect the particle radiation behaviour even though the same particle radiative property model is employed. Also, for the

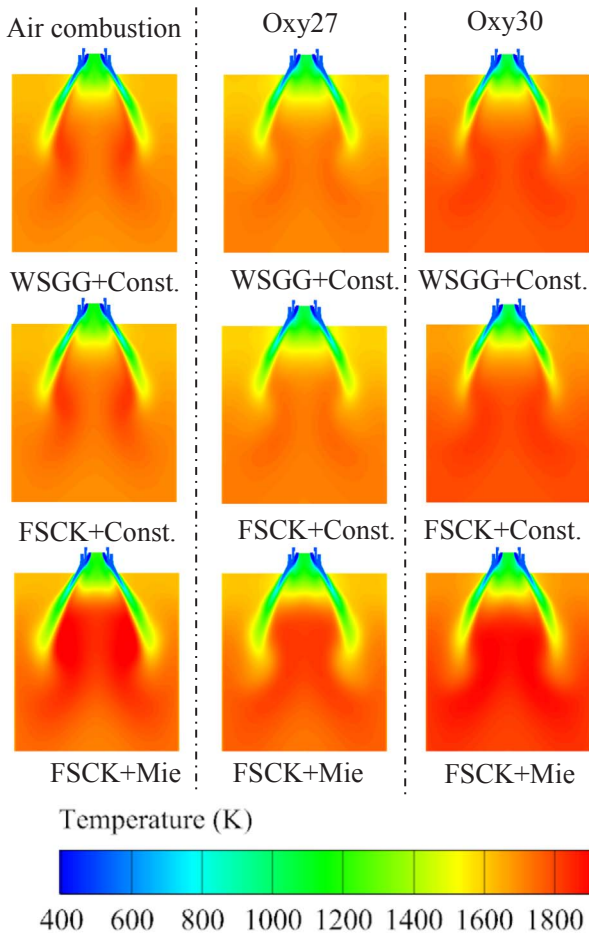


Fig. 5. Comparison of the gas temperature distributions by using different radiative property models for the air and oxyfuel cases.

investigated cases, it is found that the difference in the predicted radiation behaviours between the Mie data based particle radiation property and the constant particle radiation property are very small. This could be attributed to the predicted particle absorption coefficients when using the Mie model being coincidentally similar to those obtained when using the constant radiation property for the current cases. Generally, similar to the pilot-scale furnace, the total radiation source term (gases and particles) is reduced when using the FSCK model and the Mie data based particle radiation property.

Fig. 11 shows the calculated surface incident radiation on the middle line of the back furnace wall by using different radiative

property models. It can be found that the surface incident radiation is similar between the air and oxyfuel cases. The surface incident radiation is slightly decreased after employing the refined radiative property models (FSCK and Mie theory based data). Fig. 12 shows the total heat transfer to the membrane wall and the superheater. It can be observed that the CFD results are in reasonable agreement with the experimental data and when using the refined radiation models results there is a better prediction performance (slightly closer to the experimental data) than using the conventional methods.

4.3. Discussions on the numerical uncertainty

In this paper, the effects of using different radiation models for the spectral properties on predicting the radiation behaviours of the gas and particle phases have been investigated for air and oxyfuel combustion in both small and large scale furnaces. Reasonable agreements are obtained between the predicted results and the experimental data for the combustion and radiation behaviours. It has been found that, through using the refined radiative property models (FSCK and Mie data based method), (i) a lower predicted particle radiation source term, (ii) a hotter flame, and (iii) a closer predicted heat transfer to the experimental data are obtained, compared to the predicted results when employing the conventional methods. Particularly, it is noted that the influence of the FSCK model on predicting the gas radiation behaviour is enhanced for the large scale furnace since approximately 2–3 times in the predicted gas radiation source terms is obtained in the flame region compared to that obtained when using WSGG model. However, the difference in the predicted gas radiation source term is very small for the pilot-scale furnace between the results obtained using the FSCK model and WSGG model. In addition, the predicted radiative heat transfer is lower when using the refined radiative property models compared to the conventional methods for both furnaces.

Although the Mie data based method has been used to predict the particle radiation properties, uncertainty may still exist since the optical properties of the coal particles and fly ash particles are dependent on the particle size and ash composition [56,68]. Experimental data of the optical properties from a wide range of fuels and fly ash particles could be helpful to develop a predictive model of the particle radiation properties with more confidence [40]. It is noted that the surface incident radiation has been 20–30% overestimated for the oxyfuel combustion cases while it is better predicted in the air-fired combustion case in the pilot-scale furnace. The discrepancy in the predicted surface incident radiations could be attributed to the numerical uncertainties from the turbulence model, the combustion models, etc. Combining the refined radiation model with the combustion models for oxyfuel conditions, along with the more accurate turbulence modelling (such as large eddy simulation), should be considered as a future study in order to achieve a further improvement in the prediction of the radiative heat transfer.

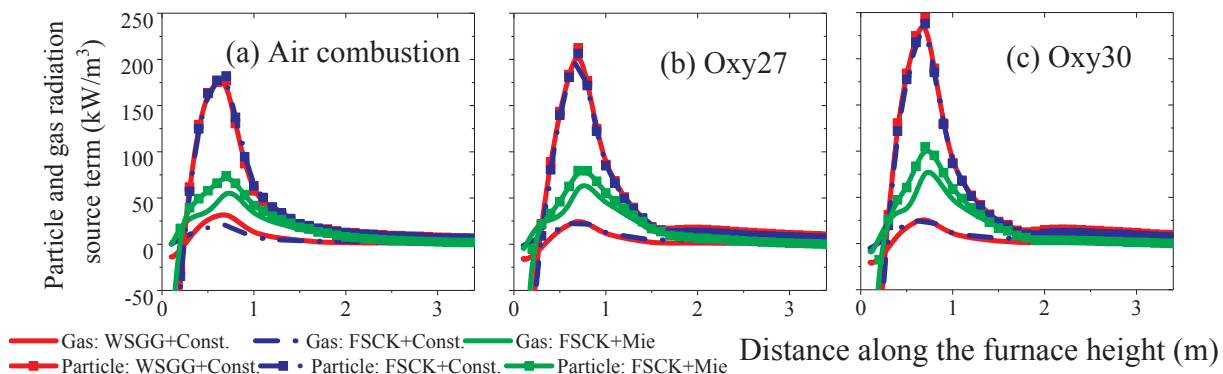


Fig. 6. Comparison of the area averaged gas and particle radiation source terms along the furnace height by using different radiative property models: (a) Air combustion, (b) Oxy27, and (c) Oxy30.

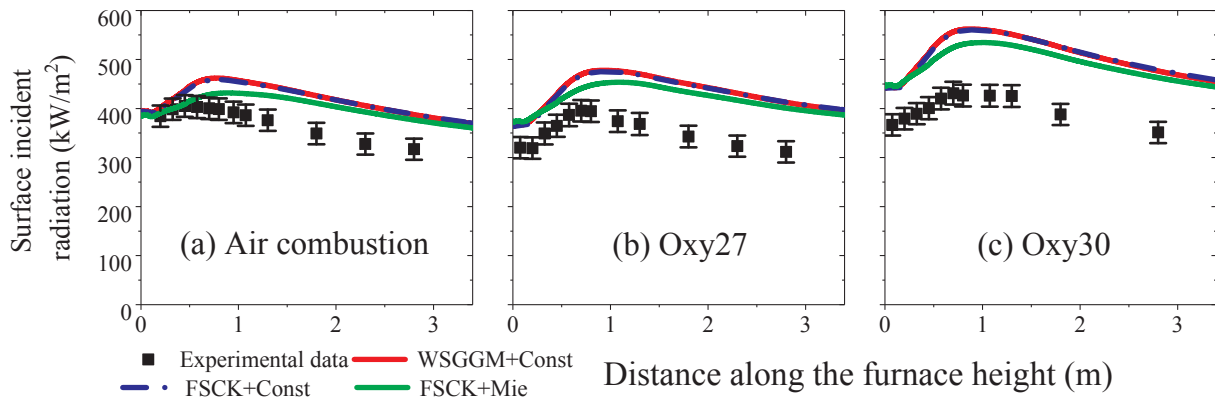


Fig. 7. Comparison of the measured and predicted surface incident radiation on the furnace wall by using different radiative property models: (a) Air combustion, (b) Oxy27, and (c) Oxy30.

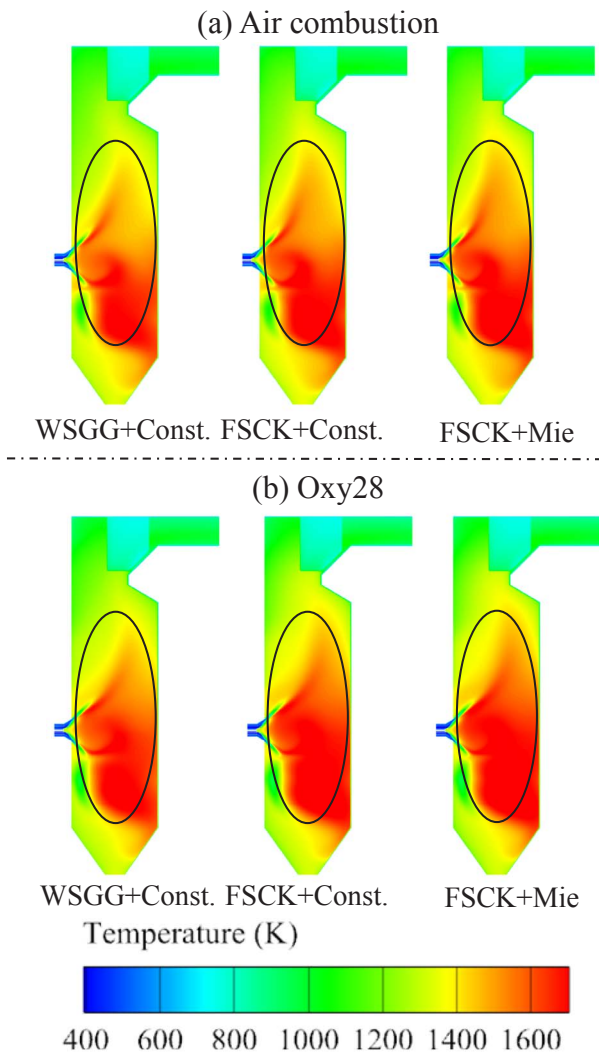


Fig. 8. Comparison of the gas temperature distribution for the air and oxyfuel cases by using different radiative property models: (a) Air combustion, and (b) Oxy28.

Turbulence modelling plays a significant role in determining the flow field, the mixing of fuel and gas and the flame properties for the pulverized coal combustion. In the current study, due to the limitation in the computational resources, the RSM turbulence model has been employed. Compared to the Large-Eddy Simulation (LES), the turbulent structures could be less accurately resolved through using the RANS method and this can correspondingly affect the predictions of the

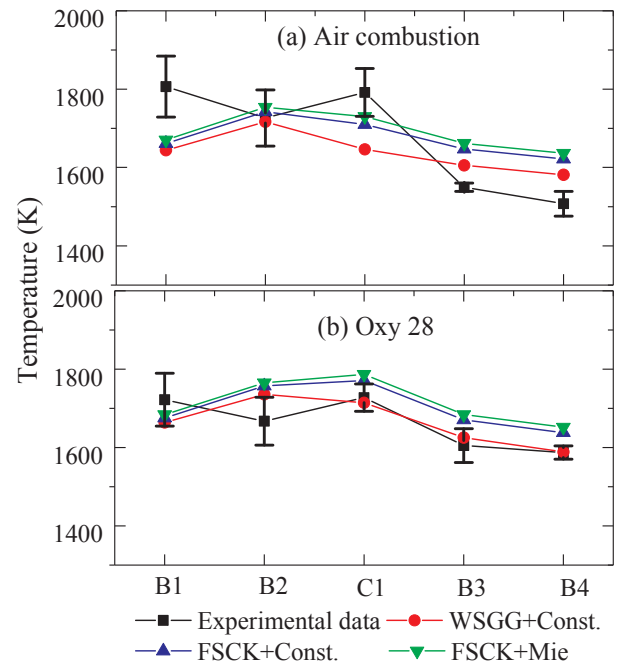


Fig. 9. Measured and predicted gas temperature at each port for the air and oxyfuel cases. Peak temperature (B1, B2 and C1) and average temperature (B3 and B4): (a) air combustion and (b) Oxy 28.

combustion and radiation behaviours. It has been found that LES is able to provide a better prediction of the flame properties (hotter temperature in the central region of the flame, smoother temperature distribution, etc.) than those by using the RANS method [10,69–71], which can correspondingly have an influence on the prediction of the radiation behaviours. However, it should be noted that the accurate prediction of the radiation behaviour by using LES is also highly dependent on the development of other sub-models (combustion models, radiation models, etc.) for simulating the pulverized coal combustion [71].

In addition to the turbulence modelling, the combustion modelling affects the prediction of the radiation behaviours. In the currently study, the same combustion models and model constants derived from the air combustion conditions have been employed for the oxyfuel combustion computations. However, char gasification reactions could be significant in the oxyfuel combustions with high CO₂ concentration. In addition, the eddy-dissipation model (EDM), which assumes that the mixing rates control the reaction rate and neglects the chemical kinetics, is employed to model the gas combustion along with the model constants empirically derived from a turbulent coal diffusion flame in a

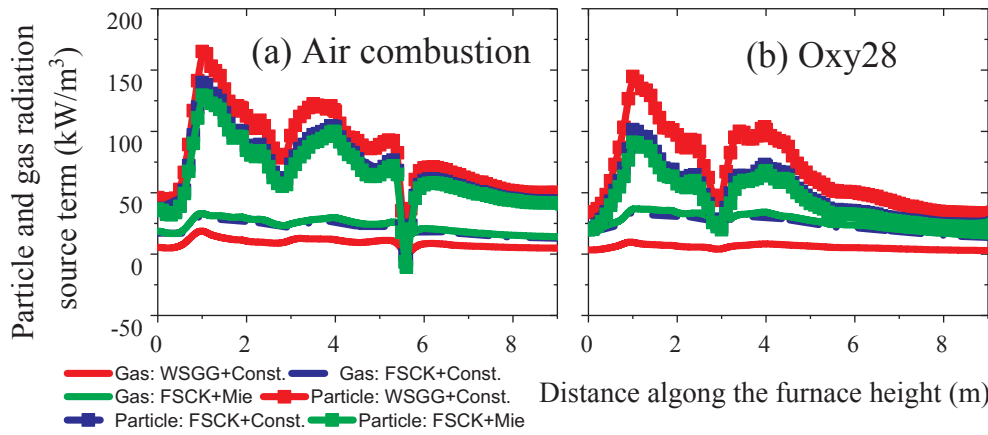


Fig. 10. Comparison of the area averaged gas and particle radiation source terms along the furnace height by using different radiative property models: (a) Air combustion and (b) Oxy28.

semi-industrial 3.4 MW furnace. The dissociation of CO₂ is neglected in EDM, while the dissociation effect could be significant in the flame region with a high temperature (especially under oxyfuel combustion), which can result in an overestimation of CO consumption rate in this study. These endothermic chemical reactions (char gasification and CO₂ dissociation) could affect the flame temperature, which can correspondingly influence the prediction of the radiation behaviours. In order to investigate the sensitivity of the combustion rate of gases on the radiation prediction, in addition to the default value (0.7) of the model constant *A* in EDM, further calculations using different values (0.125, 0.25, 0.375, and 1), which represents the combustion rate of CO gradually increasing with an increasing value of *A*, have been undertaken. Another numerical uncertainty may be attributed to the turbulent particle dispersion method, which affects the particle trajectories and hence it is possible to have an influence on the combustion and radiation behaviours. In addition to the default value (0.3) of the empirical time scale constant, *C_L*, further calculations using different values of *C_L* (no DRW, 0.15 and 0.6), which represents the particle turbulent dispersion gradually enhances with increasing the value of *C_L*, have been undertaken. As shown in Fig. 13, the predictions of the surface incident radiation is much more sensitive to the gas combustion compared with the particle turbulent dispersion when the RANS method is employed. In addition, it is observed that the surface incident radiation reduces with decreasing the CO combustion rate by reducing the value of *A* in EDM, which confirms that the less accurately modelling the gas combustion for oxyfuel conditions through using EDM in which the dissociation effect and the chemical kinetics are ignored could lead to an over prediction of the surface incident radiation. Therefore, developing robust and numerically stable gas reaction mechanisms, which take into consideration the chemical kinetics for oxy-coal combustion could potentially be significant for predicting

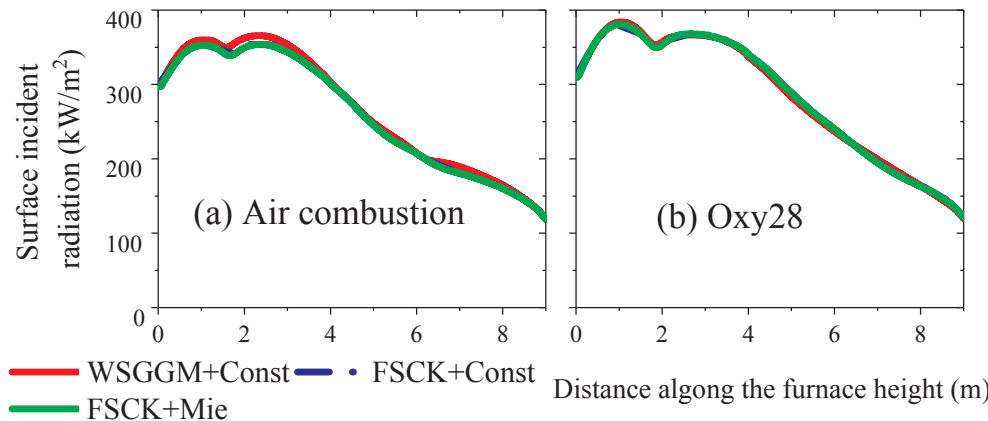


Fig. 11. Comparison of the predicted surface incident radiation on the middle line of the back furnace wall by using different radiative property models: (a) Air combustion and (b) Oxy28.

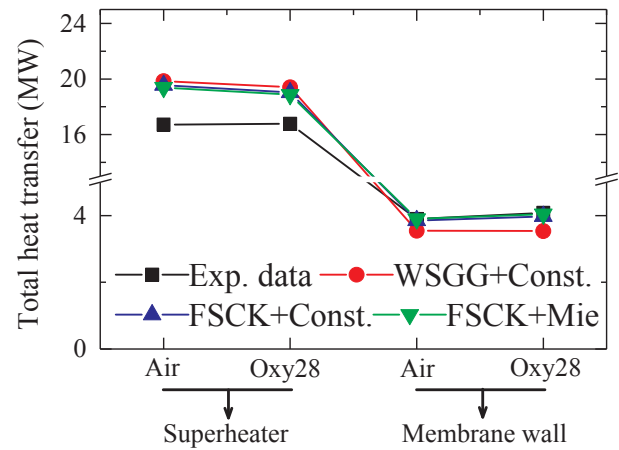


Fig. 12. Comparison of the measured and predicted total heat transfer on the membrane wall and the superheater by using different radiative property models for the air and oxyfuel cases.

combustion and radiation behaviours with confidence.

5. Conclusions

CFD modelling of coal combustion in small and large scale furnaces at air-fired and oxy-fired combustion conditions has been carried out by using refined radiation models for the spectral properties (FSCK and Mie theory based data). The predicted results for the radiation behaviours and the combustion behaviours (in-furnace gas compositions and temperatures) have been compared with the measured data from the two furnaces and reasonable agreements are obtained. Also, it can be

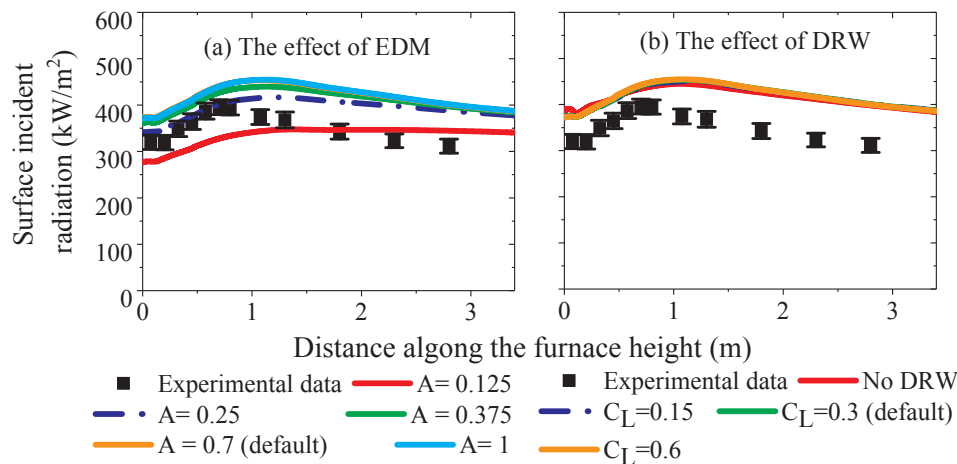


Fig. 13. The effects of eddy-dissipation model (EDM) and Discrete Random Walk (DRW) model when using different model constants on predicting the surface incident radiation: (a) the effect of EDM, and (b) the effect of DRW.

found that the similar temperature distribution and wall incident radiation under air-firing can be obtained under oxy-firing by adjusting the O₂ concentrations. The main conclusions are as follows:

- (i) The conventional use of the weighted sum of grey gases model (WSGG) and the constant values of the particle radiation properties predicts the lower gas radiation source term in the flame region. The refined radiative property models, using the full-spectrum correlated k model (FSCK) and Mie theory based data, shows a higher gas radiation source term and lower particle radiation source term in the flame region, compared to the predicted results when using the conventional methods. It is noted that the influence of the FSCK model on predicting the gas radiation behaviour is enhanced for the large scale furnace.
- (ii) The refined radiative property models predict a higher flame temperature, approximately 50–150 K in this study. This is because the predicted total radiation source term (gases and particles) reduces after using the refined models. In addition, the predicted heat transfer is closer to the experimental data by employing the refined methods. For both furnaces, the predicted surface incident radiation reduces when using the refined radiative property models. The difference in the predicted surface incident radiation between the refined radiative property models and the conventional methods is relevant with the difference in the predicted radiation properties between the two modelling techniques. The difference in the predicted surface incident radiation is relatively large (up to approximately 6% lower in the flame region) for the small scale furnace while the difference is marginal for the large scale furnace. This is because the variance in the predicted radiation source term in the small scale furnace is much higher than the variance in the large scale furnace.
- (iii) The results suggests that the refined models can be a useful tool to predict the radiation behaviours and validate other sub-models (combustion models, turbulence models, etc.) for CFD modelling of solid fuel combustion in both air and oxyfuel combustion conditions. Particularly, it is noted that gas radiation and particle radiation interact with each other through changing the temperature distributions in the furnace. The findings highlight the importance of rigorous treatments of radiation properties for both the gas and particles in order to predict the radiation behaviours for the large scale furnace with confidence.

Acknowledgment

The authors would like to acknowledge the support from the Engineering and Physical Sciences Research Council (EPSRC) grants (UKCCSRC-C2-193, Investigating the radiative heat flux in small and

large scale oxy-coal furnaces for CFD model development and system scale up). The authors also acknowledge the validation data obtained at the UKCCSRC PACT Facilities, funded by the Department for Business, Energy & Industrial Strategy (BEIS) and the Engineering and Physical Sciences Research Council (EPSRC).

References

- [1] Chen L, Yong SZ, Ghoniem AF. Oxy-fuel combustion of pulverized coal: characterization, fundamentals, stabilization and CFD modeling. *Prog Energy Combust Sci* 2012;38:156–214.
- [2] Edge P, Gharebaghi M, Irons R, Porter R, Porter RTJ, Pourkashanian M, et al. Combustion modelling opportunities and challenges for oxy-coal carbon capture technology. *Chem Eng Res Des* 2011;89:1470–93.
- [3] Wall T, Liu Y, Spero C, Elliott L, Khare S, Rathnam R, et al. An overview on oxyfuel coal combustion—state of the art research and technology development. *Chem Eng Res Des* 2009;87:1003–16.
- [4] Yin C, Yan J. Oxy-fuel combustion of pulverized fuels: combustion fundamentals and modeling. *Appl Energy* 2016;162:742–62.
- [5] Mao Z, Zhang L, Zhu X, Pan C, Yi B, Zheng C. Modeling of an oxy-coal flame under a steam-rich atmosphere. *Appl Energy* 2016;161:112–23.
- [6] Yin C. Effects of moisture release and radiation properties in pulverized fuel combustion: a CFD modelling study. *Fuel* 2016;165:252–9.
- [7] Yin C. On gas and particle radiation in pulverized fuel combustion furnaces. *Appl Energy* 2015;157:554–61.
- [8] Hu Y, Li H, Yan J. Numerical investigation of heat transfer characteristics in utility boilers of oxy-coal combustion. *Appl Energy* 2014;130:543–51.
- [9] Black S, Szuhánszki J, Pranzitelli A, Ma L, Stanger PJ, Ingham DB, et al. Effects of firing coal and biomass under oxy-fuel conditions in a power plant boiler using CFD modelling. *Fuel* 2013;113:780–6.
- [10] Clements AG, Black S, Szuhánszki J, Stechly K, Pranzitelli A, Nimmo W, et al. LES and RANS of air and oxy-coal combustion in a pilot-scale facility: predictions of radiative heat transfer. *Fuel* 2015;151:146–55.
- [11] Hu Y, Yan J. Numerical simulation of radiation intensity of oxy-coal combustion with flue gas recirculation. *Int J Greenhouse Gas Control* 2013;17:473–80.
- [12] Álvarez L, Gharebaghi M, Jones JM, Pourkashanian M, Williams A, Riaza J, et al. CFD modeling of oxy-coal combustion: prediction of burnout, volatile and NO precursors release. *Appl Energy* 2013;104:653–65.
- [13] Álvarez L, Yin C, Riaza J, Pevida C, Pis JJ, Rubiera F. Oxy-coal combustion in an entrained flow reactor: application of specific char and volatile combustion and radiation models for oxy-firing conditions. *Energy* 2013;62:255–68.
- [14] Álvarez L, Yin C, Riaza J, Pevida C, Pis JJ, Rubiera F. Biomass co-firing under oxy-fuel conditions: a computational fluid dynamics modelling study and experimental validation. *Fuel Process Technol* 2014;120:22–33.
- [15] Guo J, Liu Z, Wang P, Huang X, Li J, Xu P, et al. Numerical investigation on oxy-combustion characteristics of a 200 MWe tangentially fired boiler. *Fuel* 2015;140:660–8.
- [16] Bhuiyan AA, Naser J. Computational modelling of co-firing of biomass with coal under oxy-fuel condition in a small scale furnace. *Fuel* 2015;143:455–66.
- [17] Bhuiyan AA, Naser J. CFD modelling of co-firing of biomass with coal under oxy-fuel combustion in a large scale power plant. *Fuel* 2015;159:150–68.
- [18] Guo J, Liu Z, Huang X, Zhang T, Luo W, Hu F, et al. Experimental and numerical investigations on oxy-coal combustion in a 35 MW large pilot boiler. *Fuel* 2017;187:315–27.
- [19] Al-Abbas AH, Naser J, Dodds D. CFD modelling of air-fired and oxy-fuel combustion of lignite in a 100 KW furnace. *Fuel* 2011;90:1778–95.
- [20] Nakod P, Krishnamoorthy G, Sami M, Orsino S. A comparative evaluation of gray and non-gray radiation modeling strategies in oxy-coal combustion simulations. *Appl Therm Eng* 2013;54:422–32.

- [21] Yan L, Yue G, He B. Development of an absorption coefficient calculation method potential for combustion and gasification simulations. *Int J Heat Mass Transf* 2015;91:1069–77.
- [22] Ren T, Modest MF, Roy S. Monte Carlo simulation for radiative transfer in a high-pressure industrial gas turbine combustion chamber. In: *Proceedings of the ASME 2017 heat transfer summer conference*, July 9–12. Washington, USA; 2017. V001T02A3.
- [23] Wang C, Modest MF, He B. Improvement of full-spectrum k-distribution method using quadrature transformation. *Int J Therm Sci* 2016;108:100–7.
- [24] Grosshandler WL. Radiative heat transfer in nonhomogeneous gases: A simplified approach. *Int J Heat Mass Transf* 1980;23:1447–59.
- [25] Modest MF. The treatment of nongray properties in radiative heat transfer: from past to present. *J Heat Transfer* 2013;135:061801–61812.
- [26] Yin C. Prediction of air-fuel and oxy-fuel combustion through a generic gas radiation property model. *Appl Energy* 2017;189:449–59.
- [27] Smith TF, Shen ZF, Friedman JN. Evaluation of coefficients for the weighted sum of gray gases model. *J Heat Transfer* 1982;104:602–8.
- [28] Hottel HC, Sarofim AF. *Radiative transfer*. McGraw-Hill; 1967.
- [29] Denison MK, Webb BW. A spectral line-based weighted-sum-of-gray-gases model for arbitrary RTE solvers. *J Heat Transfer* 1993;115:1004–12.
- [30] Modest MF, Zhang H. The full-spectrum correlated-k distribution for thermal radiation from molecular gas-particulate mixtures. *J Heat Transfer* 2001;124:30–8.
- [31] Clements AG, Porter R, Pranzitelli A, Pourkashanian M. Evaluation of FSK models for radiative heat transfer under oxyfuel conditions. *J Quant Spectrosc Radiat Transfer* 2015;151:67–75.
- [32] Soufiani A, Djavdan E. A comparison between weighted sum of gray gases and statistical narrow-band radiation models for combustion applications. *Combust Flame* 1994;97:240–50.
- [33] Johansson R, Leckner B, Andersson K, Johnsson F. Account for variations in the H₂O to CO₂ molar ratio when modelling gaseous radiative heat transfer with the weighted-sum-of-grey-gases model. *Combust Flame* 2011;158:893–901.
- [34] Johansson R. Efficient treatment of non-grey radiative properties of particles and gases in modelling of radiative heat transfer in combustion environments. *Int J Heat Mass Transf* 2017;108(Part A):519–28.
- [35] Yin C, Johansen LCR, Rosendahl LA, Kær SK. New weighted sum of gray gases model applicable to computational fluid dynamics (CFD) modeling of oxy–fuel combustion: derivation, validation, and implementation. *Energy Fuels* 2010;24:6275–82.
- [36] Yin C. Refined weighted sum of gray gases model for air-fuel combustion and its impacts. *Energy Fuels* 2013;27:6287–94.
- [37] Kangwanpongpan T, França FHR, Corrêa da Silva R, Schneider PS, Krautz HJ. New correlations for the weighted-sum-of-gray-gases model in oxy-fuel conditions based on HITEMP 2010 database. *Int J Heat Mass Transf* 2012(55):7419–33.
- [38] Bordbar MH, Węcel G, Hyppänen T. A line by line based weighted sum of gray gases model for inhomogeneous CO₂–H₂O mixture in oxy-fired combustion. *Combust Flame* 2014;161:2435–45.
- [39] Modest MF, Riazzi RJ. Assembly of full-spectrum k-distributions from a narrow-band database; effects of mixing gases, gases and nongray absorbing particles, and mixtures with nongray scatterers in nongray enclosures. *J Quant Spectrosc Radiat Transfer* 2005;90:169–89.
- [40] Clements AG. *Modelling mercury oxidation and radiative heat transfer in oxy-coal environments* [Doctoral thesis]. University of Leeds; 2016.
- [41] Porter R, Liu F, Pourkashanian M, Williams A, Smith D. Evaluation of solution methods for radiative heat transfer in gaseous oxy-fuel combustion environments. *J Quant Spectrosc Radiat Transfer* 2010;111:2084–94.
- [42] Chu H, Gu M, Consalvi J-L, Liu F, Zhou H. Effects of total pressure on non-grey gas radiation transfer in oxy-fuel combustion using the LBL, SNB, SNBCK, WSGG, and FSK methods. *J Quant Spectrosc Radiat Transfer* 2016;172:24–35.
- [43] Johansson R, Leckner B, Andersson K, Johnsson F. Influence of particle and gas radiation in oxy-fuel combustion. *Int J Heat Mass Transf* 2013;65:143–52.
- [44] Zhang J, Ito T, Ito S, Riechelmann D, Fujimori T. Numerical investigation of oxy-coal combustion in a large-scale furnace: Non-gray effect of gas and role of particle radiation. *Fuel* 2015;139:87–93.
- [45] Black AJ. *Oxy-fuel combustion for carbon capture using computational fluid dynamics* [Doctoral thesis]. University of Leeds; 2014.
- [46] Szuhanzski J. *Advanced oxy-fuel combustion for carbon capture and sequestration* [Doctoral thesis]. University of Leeds; 2014.
- [47] Gibson MM, Launder BE. Ground effects on pressure fluctuations in the atmospheric boundary layer. *J Fluid Mech* 2006;86:491–511.
- [48] Ansys. *15.0 Theory Guide* 2013.
- [49] German AE, Mahmud T. Modelling of non-premixed swirl burner flows using a Reynolds-stress turbulence closure. *Fuel* 2005;84:583–94.
- [50] Gran IR, Ertesvag IS, Magnussen BF. Influence of turbulence modeling on predictions of turbulent combustion. *AIAA J* 1997;35:106–10.
- [51] Weber R, Visser BM, Boysan F. Assessment of turbulence modeling for engineering prediction of swirling vortices in the near burner zone. *Int J Heat Fluid Flow* 1990;11:225–35.
- [52] Boulet P, Collin A, Consalvi JL. On the finite volume method and the discrete ordinates method regarding radiative heat transfer in acute forward anisotropic scattering media. *J Quant Spectrosc Radiat Transfer* 2007;104:460–73.
- [53] Mazumder S, Modest MF. Application of the full spectrum correlated-k distribution approach to modeling non-gray radiation in combustion gases. *Combust Flame* 2002;129:416–38.
- [54] Bohren CF, Huffman DR. *Absorption and scattering of light by small particles*. John Wiley & Sons; 2008.
- [55] Manickavasagam S, Menguc MP. Effective optical properties of pulverized coal particles determined from FT-IR spectrometer experiments. *Energy Fuels* 1993;7:860–9.
- [56] Goodwin DG, Mitchner M. Measurements of the near infrared optical properties of coal slags. *Chem Eng Commun* 1986;44:241–55.
- [57] Liu F, Swithenbank J. The effects of particle size distribution and refractive index on fly-ash radiative properties using a simplified approach. *Int J Heat Mass Transf* 1993;36:1905–12.
- [58] Xu K, Wu Y, Shen H, Zhang Q, Zhang H. Predictions of soot formation and its effect on the flame temperature of a pulverized coal-air turbulent jet. *Fuel* 2017;194:297–305.
- [59] Brown AL, Fletcher TH. Modeling soot derived from pulverized coal. *Energy Fuels* 1998;12:745–59.
- [60] Li G, Modest MF. Importance of turbulence-radiation interactions in turbulent diffusion jet flames. *J Heat Transfer* 2003;125:831–8.
- [61] Li G, Modest MF. Application of composition PDF methods in the investigation of turbulence–radiation interactions. *J Quant Spectrosc Radiat Transfer* 2002;73:461–72.
- [62] Yang X, Ingham D, Ma L, Zhou H, Pourkashanian M. Understanding the ash deposition formation in Zhundong lignite combustion through dynamic CFD modelling analysis. *Fuel* 2017;194:533–43.
- [63] Yang X, Ingham D, Ma L, Williams A, Pourkashanian M. Predicting ash deposition behaviour for co-combustion of palm kernel with coal based on CFD modelling of particle impaction and sticking. *Fuel* 2016;165:41–9.
- [64] Shirokhar JS, Coimbra CFM, Queiroz McQuay M. Fundamental aspects of modeling turbulent particle dispersion in dilute flows. *Prog Energy Combust Sci* 1998;22:363–99.
- [65] Gouesbet G, Berlemont A. Eulerian and Lagrangian approaches for predicting the behaviour of discrete particles in turbulent flows. *Prog Energy Combust Sci* 1999;25:133–59.
- [66] Magnussen BF, Hjertager BH. On mathematical modeling of turbulent combustion with special emphasis on soot formation and combustion. *Symp (Int) Combust* 1977;16:719–29.
- [67] Visser BM, Smart JP, De Van, Kamp WL, Weber R. Measurements and predictions of swirl zone properties of swirling pulverised coal flames. *Symp (Int) Combust* 1991;23:949–55.
- [68] Johansson R, Gronarz T, Kneer R. Influence of index of refraction and particle size distribution on radiative heat transfer in a pulverized coal combustion furnace. *J Heat Transfer* 2017;139:042702–42708.
- [69] Gharebaghi M, Irons RMA, Ma L, Pourkashanian M, Pranzitelli A. Large eddy simulation of oxy-coal combustion in an industrial combustion test facility. *Int J Greenhouse Gas Control* 2011;5(Supplement 1):S100–10.
- [70] Warzecha P, Boguslawski A. Simulations of pulverized coal oxy-combustion in swirl burner using RANS and LES methods. *Fuel Process Technol* 2014;119:130–5.
- [71] Edge P, Gubba SR, Ma L, Porter R, Pourkashanian M, Williams A. LES modelling of air and oxy-fuel pulverised coal combustion—impact on flame properties. *Proc Combust Inst* 2011;33:2709–16.